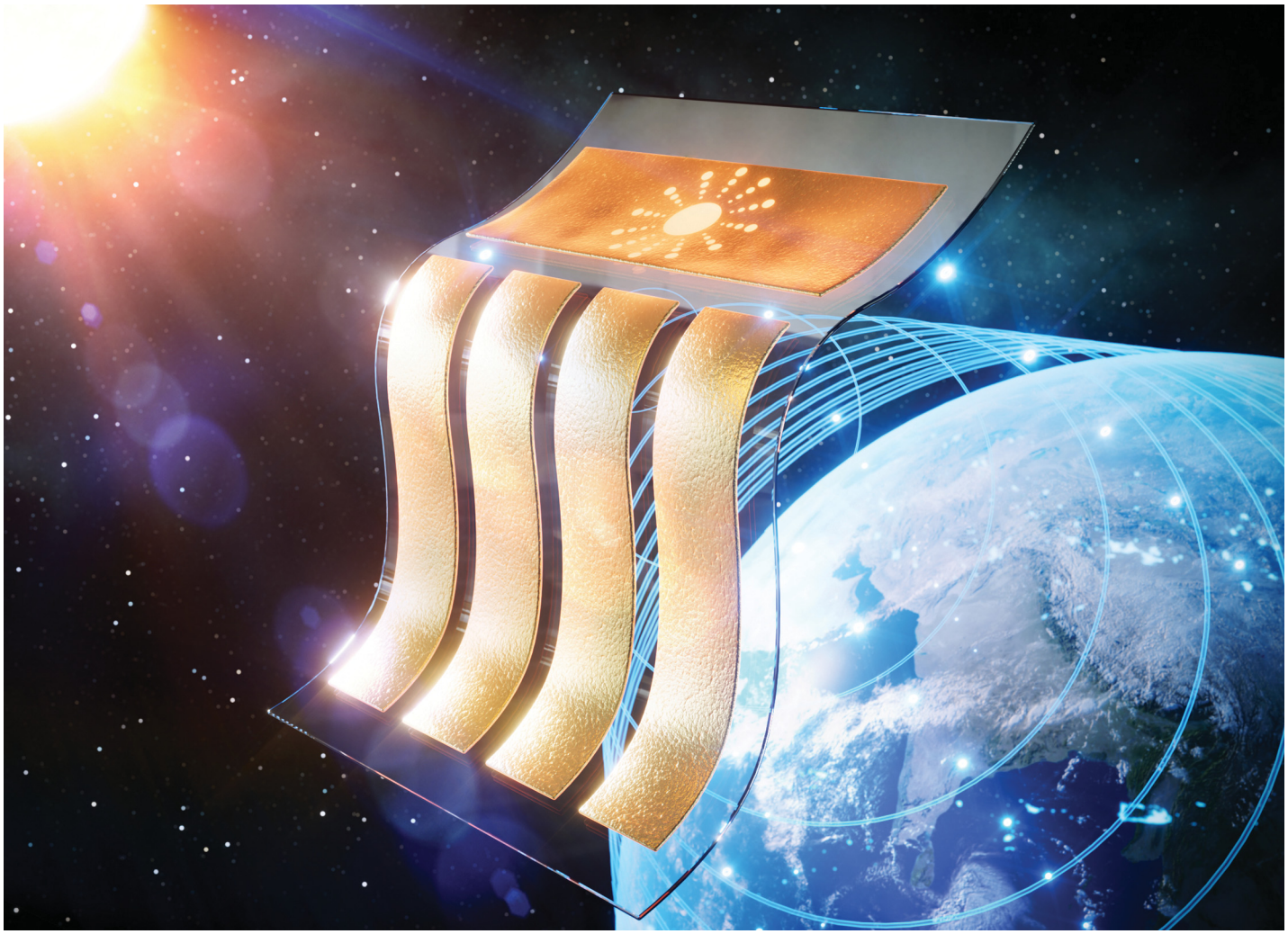

Showcasing research from Professor Bumjoon Kim's laboratory, KAIST, and Yun-Hi Kim's laboratory, GNU, Republic of Korea.

Trimerized small-molecule acceptors enable high-performance organic solar cells with high open-circuit voltage and prolonged life-time

Small-molecule acceptors (SMAs) have led to remarkable advances in the power conversion efficiencies (PCEs) of organic solar cells (OSCs), but the resulting OSCs typically have poor long-term stability. Herein, we develop a new trimer acceptor (TYT), consisting of three Y-based molecules linked by thiophene spacers. The TYT-based OSCs demonstrate high-performance (PCE = 18.2%) and excellent photostability ($t_{80\%}$ lifetime > 8000 h), which outperform those of the OSCs based on the monomer (MYT, PCE = 16.4% and $t_{80\%}$ lifetime = 35 h) and dimer acceptors (DYT, PCE = 17.3% and $t_{80\%}$ lifetime = 2551 h).

As featured in:

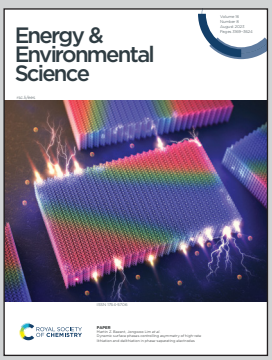

See Bumjoon J. Kim *et al.*, *Energy Environ. Sci.*, 2023, **16**, 3339.

ROYAL SOCIETY OF CHEMISTRY

rsc.li/ees

Registered charity number: 207890

Energy & Environmental Science

ROYAL SOCIETY OF CHEMISTRY

PAPER

View Article Online
View Journal | View Issue

Cite this: *Energy Environ. Sci.*, 2023, **16**, 3339

Trimerized small-molecule acceptors enable high-performance organic solar cells with high open-circuit voltage and prolonged life-time†

Jin-Woo Lee,‡[a] Cheng Sun,‡[bc] Tan Ngoc-Lan Phan,[a] Dong Chan Lee,[d] Zhengping Tan,[a] Hyesu Jeon,[a] Shinuk Cho,[d] Soon-Ki Kwon,[e] Yun-Hi Kim *[c] and Bumjoon J. Kim *[a]

Although the recent development of Y-series small-molecule acceptors (SMAs) has led to a dramatic increase in the power conversion efficiency (PCE) of organic solar cells (OSCs), the operational stability (device lifetime) of OSCs is inadequate for commercialization. In this study, we develop a new trimer acceptor (TYT), consisting of three Y-based molecules linked by electron-donating spacers, to realize an OSC with high-performance (PCE > 18%) and -stability ($t_{80\%}$ lifetime > 8000 h under 1 sun illumination, in which $t_{80\%}$ lifetime is the time required for the PCE of the OSC to reach 80% of its initial value). We demonstrate that the trimerization approach affords an acceptor, TYT, with an upshifted lowest unoccupied molecular orbital energy level, which, in turn, affords an efficient OSC with a high open-circuit voltage (0.964 V). In addition, the glass-transition temperature (T_g) of TYT (217 °C) is significantly higher than those of monomer (MYT, T_g = 80 °C) and dimer (DYT, T_g = 127 °C) acceptors, which effectively suppresses the molecular diffusion of TYT in a blend film with a polymer donor. Accordingly, a TYT-based OSC demonstrates a high PCE (18.2%) and long $t_{80\%}$ lifetime under 1 sun illumination (8454 h), outperforming MYT- and DYT-based OSCs that exhibit PCEs and $t_{80\%}$ lifetimes of 16.4% and 35 h, and 17.3% and 2551 h, respectively. Therefore, this study provides important guidelines for the design of electron acceptors in achieving OSCs with high performance and stability close to a commercial level.

Received 28th January 2023,
Accepted 26th May 2023

DOI: 10.1039/d3ee00272a

rsc.li/ees

Broader context

High power conversion efficiency (PCE) and long-term stability are important requirements for commercialization of organic solar cells (OSCs). Small-molecule acceptors (SMAs) are the core materials that have led to remarkable advances in the PCEs of the OSCs, but the resulting OSCs typically have poor long-term stability. The low glass transition temperatures (T_gs) and rapid diffusion of SMAs owing to their small molecular sizes are recognized as the main causes of the poor stability of OSCs. In addition, the PCEs of OSCs are still lower than those of other types of photovoltaic devices, such as perovskite solar cells, mainly because of their relatively low open-circuit voltage (V_{oc} < 0.90 V). To address these performance limitations, we develop a new trimer acceptor (TYT), consisting of three Y-based molecules linked by electron-donating thiophene spacers. The TYT-based OSCs demonstrate high-performance (V_{oc} = 0.964 V and PCE = 18.15%) and excellent photo-stability ($t_{80\%}$ lifetime > 8000 h), which outperform those of the OSCs based on the monomer (MYT, PCE = 16.44% and $t_{80\%}$ lifetime = 35 h) and dimer acceptors (DYT, PCE = 17.29% and $t_{80\%}$ lifetime = 2551 h).

[a] *Department of Chemical and Biomolecular Engineering, Korea Advanced Institute of Science and Technology (KAIST), Daejeon 34141, Republic of Korea. E-mail: bumjoonkim@kaist.ac.kr*
[b] *Qingdao Institute of Bioenergy and Bioprocess Technology, Chinese Academy of Sciences, Qingdao, 266101, China*
[c] *Department of Chemistry and RINS, Gyeongsang National University, Jinju 52828, Republic of Korea. E-mail: ykim@gnu.ac.kr*
[d] *Department of Physics and EHSRC, University of Ulsan, Ulsan 44610, Republic of Korea*
[e] *Department of Materials Engineering and Convergence Technology and ERI, Gyeongsang National University, Jinju 52828, Republic of Korea*

† Electronic supplementary information (ESI) available: Cyclic voltammogram, UV-Vis spectra, additional GIWAXS analysis, and DM_T analysis) and experimental procedures. See DOI: https://doi.org/10.1039/d3ee00272a

‡ J.-W. Lee and C. Sun contributed equally to this work.

Introduction

The rapid increase in the power conversion efficiency (PCE) of organic solar cells (OSCs) to 18–19%, is ascribed to the development of efficient polymer donors and non-fullerene small-molecule acceptors (SMAs).[1–10] However, numerous SMA-based OSCs exhibit poor operation stabilities under thermal stress and light-illumination, mainly due to the unstable, kinetically trapped blend morphologies of their active layers, *i.e.*, blends of polymer donors and SMAs.[11–15] Due to their small size, SMAs (which typically have low glass-transition temperature (T_g < 100 °C) and high diffusion coefficient ($D > 10^{-20}$ cm^2 s^{-1} at 85 °C)) in these active layers readily diffuse under thermal stress, resulting in phase separation.[16–18] In comparison, polymerized small-molecule-acceptors (PSMAs) typically have higher T_g and lower D than SMAs due to larger molecular sizes. Thus, PSMA-based OSCs often exhibit improved device stabilities and mechanical robustness.[12,19–33] However, PSMA-based OSCs often show lower electron mobility and, therefore, lower PCE than SMA-based OSCs as polydisperse chains of the PSMAs suppress the formation of regular and tight packing in films, resulting in comparably less-ordered intermolecular assemblies.

Recently, dimerized small-molecule acceptors (DSMAs) have garnered attention as they can leverage the advantages of both SMAs and PSMAs.[34–37] DSMAs demonstrate higher electron mobility than PSMAs because their discrete molecular structures can promote regular and tight packing.[38–41] In addition, the T_gs and Ds of DSMAs are higher and lower, respectively, than those of SMAs, owing to their comparatively large size; these properties lead to OSCs with enhanced thermal and photo-stability. Wang *et al.* were the first to develop a DSMA featuring Y-series-based building blocks (dBTICγ-EH) to realize an OSC with a high PCE (16.06%) and operational stability ($t_{80\%}$ lifetime; 1020 h).[37] Subsequently, researchers developed DSMA-based OSCs with PCEs exceeding 18% and high stability ($t_{80\%}$ lifetimes > 1000 h) through the judicious selection of electron-donating spacers to link the SMA building blocks of the DSMAs.[34]

Despite the demonstrated potential of DSMA systems, the stability of the OSCs remains a challenge; the operational stability of the DSMA-based OSCs falls short of the commercial requirement, *i.e.*, the device lifetime is less than the required minimum of 5 years.[42–44] This limitation necessitates the development of novel acceptors using a rational molecular design approach. Recent studies concerning DSMAs imply that to realize stable OSCs with long operational lifetimes, acceptors must have high T_gs (>200 °C) and low D_{85} (<10^{-24} cm^2 s^{-1} at 85 °C).[16–18] Accordingly, we anticipate that a trimer acceptor will demonstrate such properties, owing to its greater molecular size (relative to that of DSMAs), and afford OSCs with longer operational lifetimes.[45–50] The proposed trimerization approach may offer an additional handle for tuning the structures of molecules and expand the library of potential electron acceptors. Moreover, this approach allows for the increased flexibility in the design of the materials with tuned energy levels and enhanced light absorbance.[46,49–51] For instance, unlike DSMAs and SMAs, which incorporate one or zero electron-donating linkers, respectively, trimer acceptors incorporate two electron-donating linkers. Thus, the trimer acceptors can have upshifted energy levels of the lowest unoccupied molecular orbital (LUMO) relative to those of corresponding SMAs and DSMAs, which may lead to OSCs with a higher open-circuit voltage (V_{oc}) and PCE. Hence, trimer acceptors can address a critical limitation of OSCs, *i.e.*, low V_{oc} (<0.9 V) relative to that of other types of solar cells (*e.g.*, perovskite solar cells with V_{oc} > 1.0 V).[52–57]

In this study, we synthesize a new trimer acceptor (TYT) consisting of three SMA units linked by two electron-donating thiophene spacers. Using TYT, we realize OSCs with a high PCE (18.15%) and excellent operational stability under 1 sun illumination ($t_{80\%}$ lifetime = 8454 h). To investigate the origin of the high efficiency and stability of the TYT-based OSCs, we also prepare and consider corresponding monomer and dimer acceptors (MYT and DYT, respectively) to establish the molecular structure–acceptor property–device performance relationship. We observe that the LUMO energy levels of the acceptors increase in the order of MYT (−4.04 eV) < DYT (−3.94 eV) < TYT (−3.86 eV), owing to the increase in the number of their electron-donating thiophene linkers. As a result, the V_{oc}s of associated OSCs increase in the same order (in terms of their acceptors), accounting for the corresponding trend in their PCEs; the V_{oc}s and PCEs of the MYT-, DYT-, and TYT-based OSCs are 0.917 V and 16.44%, 0.942 V and 17.29%, and 0.964 V and 18.15%, respectively. In addition, the extended molecular structure of the trimer acceptor accounts for the excellent operational stability of the TYT-based OSCs. TYT is found to have a significantly higher T_g of 217 °C and lower D_{85} of 1.44 × 10^{-25} cm^2 s^{-1}, respectively, compared to those of MYT (T_g = 80 °C and D_{85} = 1.21 × 10^{-16} cm^2 s^{-1}) and DYT (T_g = 127 °C and D_{85} = 1.05 × 10^{-19} cm^2 s^{-1}). The high T_g and low D of TYT afford an OSC with excellent device stability under illumination. For example, the $t_{80\%}$ lifetime of the TYT-based OSC (8454 h) is significantly longer than those of the MYT- and DYT-based OSCs (35 and 2551 h, respectively). Thus, our results highlight the great potential of the trimer acceptor system for realizing stable, high-performance OSCs.

Results and discussion

To investigate the relationship between the molecular structures of acceptors of different size, their properties, and OSC performance, we synthesized a series of electron acceptors, *i.e.*, monomer, dimer, and trimer acceptors (MYT, DYT, and TYT, respectively) (Fig. 1(a)). We prepared an asymmetric Y-series-based compound with a dichlorinated 1,1-dicyanomethylene-3-indanone (IC) group at one end and a brominated IC group at the other (compound **2**, Scheme S1, ESI†); this compound was dimerized by the Stille coupling reaction with bis(trimethyltin)-functionalized thiophene (Th–SnMe$_3$) monomers to produce DYT (Fig. 1(a) and Scheme S3, ESI†). We also prepared a Y-series–based compound with two brominated IC end units (compound **3**). The trimer acceptor, TYT, was synthesized by two-step reactions using the three monomers of compound **2**, compound **3**, and Th–SnMe$_3$

(Fig. 1(a) and Scheme S4, ESI†). Compound **3** and Th–$SnMe_3$ firstly reacted by the Stille coupling for 3 h. Then, compound **2** was sequentially added during the reaction, and the coupling continued for additional 10 h. The synthetic and purification procedures are detailed in the ESI.†

The chemical structures of the acceptors (MYT, DYT, and TYT) and their intermediates were confirmed by nuclear magnetic resonance (NMR) spectroscopy (Fig. S1–S5, ESI†). The discrete molecular weights of MYT, DYT, and TYT were determined by matrix-assisted laser desorption/ionization time-of-flight (MALDI-ToF) mass spectrometry, which confirm the successful synthesis of pure acceptor materials (Fig. S6, ESI†). The determined molar masses of MYT, DYT, and TYT were 1881, 3712, and 5540 g mol^{-1}, respectively. Based on optimized structures from density functional theory (DFT) calculations, the dihedral angles near the IC units of all the acceptors were found to be less than 16°, which indicates that the molecules adopt relatively planar molecular conformations (Fig. S7, ESI†).

We investigated the electrochemical properties of the synthesized acceptors using cyclic voltammetry (CV) (Fig. S8, ESI† and Table 1). The LUMO energy levels of the acceptors were linearly upshifted with increasing molecular size; MYT (−4.04 eV) < DYT (−3.94 eV) < TYT (−3.86 eV). The upshifted LUMO energy level of TYT leads to an OSC with a comparatively high V_{oc}. The respective LUMO and highest occupied molecular orbital (HOMO) energy levels of the three acceptors align appropriately with those of the polymer donor, poly[(2,6-(4,8-bis(5-(2-ethylhexyl-3-fluoro)thiophene-2-yl)-benzo[1,2-*b*:4,5-*b*′]dithiophene))-*alt*-(5,5-(1′,3′-di-2-thienyl-5′,7′-bis(2-ethylhexyl)benzo[1′,2′-*c*:4′,5′-*c*′]dithiophene-4,8-dione)] (PM6), used in this study (Fig. 1(b)).

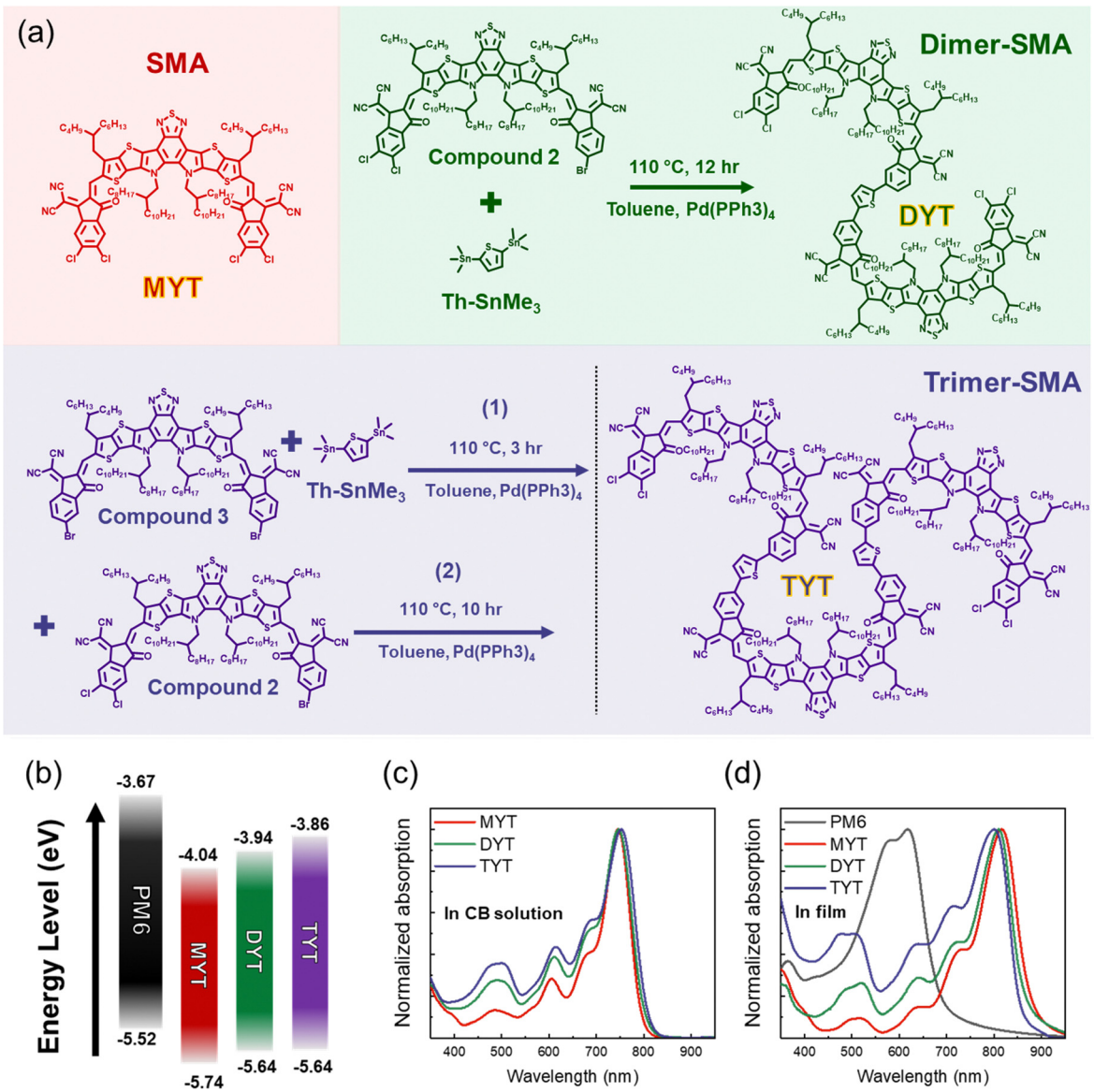

Fig. 1 (a) Chemical structures and synthetic procedures, (b) energy levels, and (c), (d) UV-Vis absorption spectra in (c) solution (CB) and (d) film of the materials used in this study.

Table 1 Optical and electrochemical properties of PM6 and electron acceptors

Material	λ_{max}^{sol} [a] (nm)	λ_{max}^{film} [b] (nm)	ε_{max}^{film} [c] ($\times 10^5$ cm^{-1})	E_{LUMO} [d] (eV)	E_{HOMO} [d] (eV)
PM6	—	621	0.79	−3.67	−5.52
MYT	745	816	1.54	−4.04	−5.74
DYT	745	809	1.62	−3.94	−5.64
TYT	745	802	1.60	−3.86	−5.64

[a] Wavelength of maximum UV-Vis absorbance (λ_{max}) in solution. [b] Wavelength of maximum UV-Vis absorbance (λ_{max}) in film. [c] Maximum absorption coefficients in film UV-Vis absorbances. [d] Measured by cyclic voltammetry.

Although the wavelengths at maximum ultraviolet-visible (UV-Vis) absorption (λ_{max}s) of all the acceptors in chlorobenzene (CB) were similar (Fig. 1(c)), their λ_{max}s in film slightly blue-shifted (decreased) in the order of MYT (λ_{max}^{film}: 816 nm), DYT (λ_{max}^{film}: 809 nm), and TYT (λ_{max}^{film}: 802 nm; Fig. 1(d)). The maximum absorption coefficients of the three acceptors in film (ε_{max}^{film}s) were similar, *i.e.*, in the range of 1.54–1.62 $\times$ 10^5 cm^{-1}.

The aggregation behavior of the acceptors in solution was analyzed by investigating their temperature-dependent UV-Vis absorbance in CB in the temperature range of 20–100 °C (Fig. 2(a)–(c)). The UV-Vis absorbance of MYT and DYT decreased with increasing solution temperature (Fig. 2(a) and (b)), suggesting that the tendency of MYT and DYT molecules to aggregate decreases with increasing temperature. In contrast, the UV-Vis absorbance of TYT did not decrease with increasing temperature to 100 °C (Fig. 2(c)), suggesting that the TYT molecules aggregate more readily at high temperatures than the MYT and DYT molecules.

The crystalline properties of the acceptors were investigated by grazing incidence wide angle X-ray scattering (GIWAXS) (Fig. 2(d)–(h), Fig. S9 and Table S1, ESI†). MYT, in film, preferred an edge-on molecular packing orientation as indicated by the 2D GIWAXS patterns showing distinct (100) and (010) peaks in the out-of-plane (OOP) and in-plane (IP) directions, respectively (Fig. 2(e)). In contrast, PM6, DYT, and TYT preferred a face-on molecular packing orientation as indicated by (100) and (010) peaks in the IP and OOP directions, respectively (Fig. 2(d), (f), and (g)). Pole figures of the MYT, DYT, and TYT acceptors were obtained from the (010) peaks in the GIWAXS results to assess the molecular packing orientation

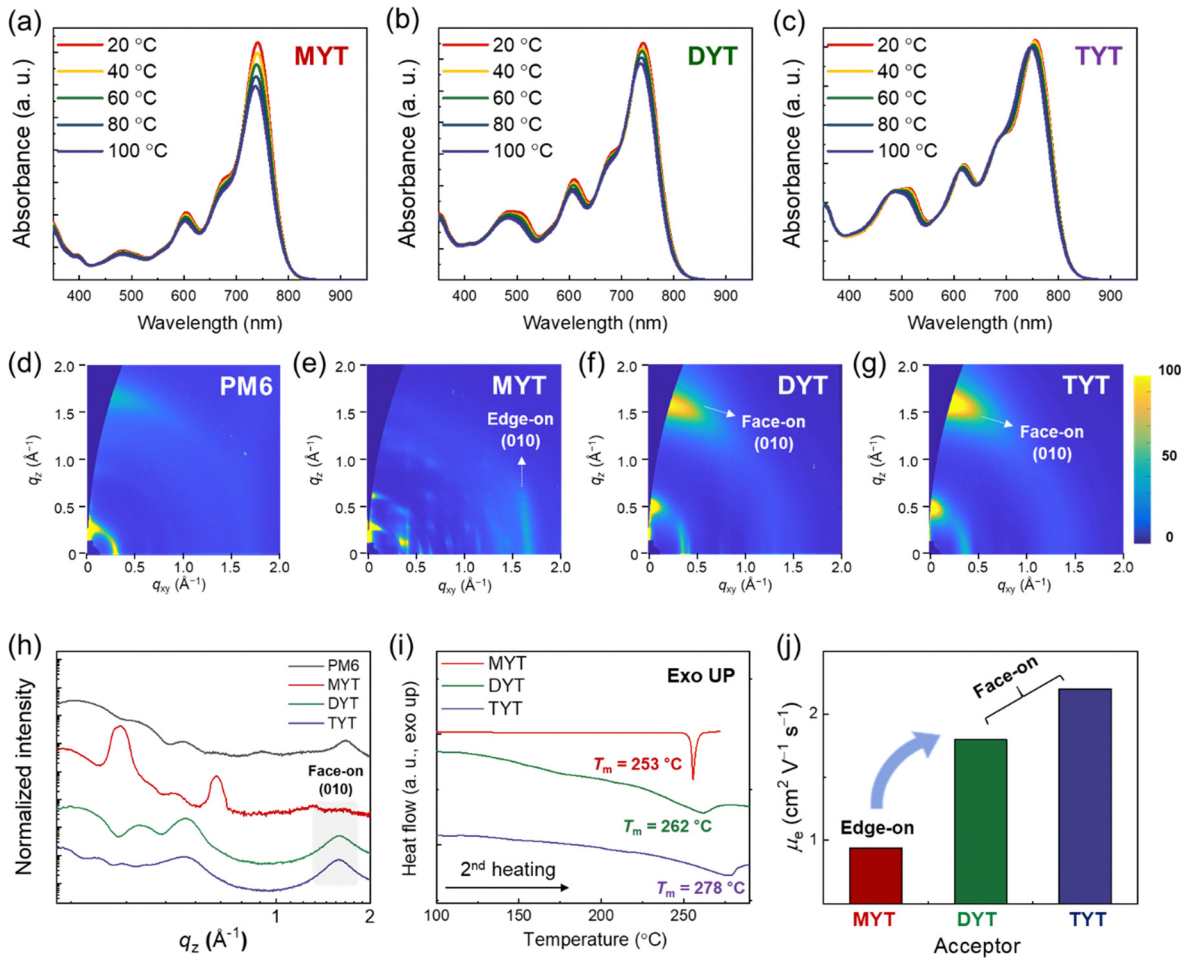

Fig. 2 (a)–(c) Temperature-dependent UV-Vis absorption spectra of (a) MYT, (b) DYT, and (c) TYT. (d)–(g) 2D GIWAXS patterns of (d) PM6, (e) MYT, (f) DYT, and (g) TYT. (h) GIWAXS linecut profiles in the OOP direction, (i) DSC curves (2nd heating cycles), and (j) SCLC electron mobility of the pristine constituents.

(Fig. S10, ESI†). The thermal properties of the acceptors were analyzed by differential scanning calorimetry (DSC). The DSC curves (2nd heating cycles) of MYT, DYT, and TYT showed transition peaks corresponding to melting, at temperatures exceeding 200 °C (Fig. 2(i)). The melting temperatures (T_ms) of the acceptors increased with increasing molecule size; MYT (T_m = 253 °C) < DYT (T_m = 262 °C) < TYT (T_m = 277 °C). The electrical properties of the acceptors in film were investigated by performing space-charge limited current (SCLC) mobility measurements (Fig. 2(j) and Table S2, ESI†).[58] The determined electron mobilities (μ_es) of DYT and TYT were significantly higher than that of MYT. This is attributed to the face-on oriented packing structures of DYT and TYT which, unlike the edge-on oriented packing structures of MYT, facilitate charge transport in the vertical direction.[59,60] Overall, the TYT showed the highest degree of aggregation and highest μ_e among the three acceptors.

We then investigated the photovoltaic performance of the acceptors by fabricating OSCs with a normal-type device structure; the OSC fabrication procedures and conditions are detailed in the ESI.† The *J*–*V* curves of the OSCs are shown in Fig. 3(a). The PCEs of the OSCs increased, in terms of the blend films, in the order of PM6:MYT (PCE = 16.44%), PM6:DYT (PCE = 17.29%), and PM6:TYT (PCE = 18.15%). The parameter mainly accounting for the difference in PCE was V_{oc}, which increased in the order of PM6:MYT (V_{oc} = 0.917 V), PM6:DYT (V_{oc} = 0.942 V), and PM6:TYT (V_{oc} = 0.964 V) (Table 2). The high V_{oc}s of the PM6:DYT and PM6:TYT OSCs are attributed to their relatively high LUMO energy levels. We note that the PM6:TYT OSCs demonstrate the highest V_{oc} (0.964 V) among reported high-performance (PCE > 18%) OSCs (Fig. S11 and Table S3, ESI†). In addition, we fabricated OSCs using three acceptors (MYT, DYT, and TYT) in combination with different donor pairs (D18, D18-Cl, and PBQx-TF). Our findings showed that the V_{oc} increased sequentially for the devices using MYT, DYT, and TYT acceptors, as listed in Table S4 (ESI†). The short-circuit current densities (J_{sc}s) of the OSCs increased in the same order as their PCEs and V_{oc}s. The fill factor (FF) of the PM6:TYT OSCs (0.75) was slightly higher than those of the PM6:MYT and PM6:DYT OSCs (0.74). PCEs of the OSCs show Gaussian distributions with small PCE deviations, indicating that the OSCs are reproducible (Fig. 3(b)). The external quantum efficiency (EQE) spectra of the OSCs are shown in Fig. 3(c), and the J_{sc}s calculated from the EQE spectra are consistent with the measured device J_{sc}s (Table 2).

We characterized the electrical properties of the OSCs to elucidate the trends in their photovoltaic performance. The voltage loss (V_{loss}) of the OSCs was measured using Fourier-transform photocurrent spectroscopy (FTPS)-EQE and electroluminescence (EL) spectroscopy to analyze the high V_{oc} of the PM6:TYT OSCs (Fig. 3(d) and Fig. S12–S14, ESI†). The V_{loss} of OSCs can be expressed in terms of ΔE_1, ΔE_2, and ΔE_3; $V_{loss}^{total} = (E_g^{PV}/q - V_{oc}^{SQ}) + (V_{oc}^{SQ} - V_{oc}^{rad}) + (V_{oc}^{rad} - V_{oc}^{PV}) = \Delta E_1 + \Delta E_2 + \Delta E_3$, where q, E_g^{PV}, V_{oc}^{SQ}, V_{oc}^{rad}, and V_{oc}^{PV} are the elementary charge, photovoltaic bandgap, maximum voltage in the Shockley–Queisser limit, voltage in radiative limit, and photovoltaic V_{oc}, respectively (Fig. S12, ESI†).[41,61,62] ΔE_1 is the intrinsic V_{loss} of the OSCs within a range of 0.20–0.30 eV. ΔE_2 is the radiative recombination loss from the tail energy states below the bandgap. ΔE_3 is the non-radiative V_{loss}, caused by non-radiative recombination in the OSCs. Detailed procedures for the calculation of V_{loss} are provided in the Experimental Section. The V_{loss}^{total} of the OSCs decreased in the order of PM6:MYT (0.516 V), PM6:DYT (0.503 V), and PM6:TYT (0.492 V) (Fig. 3(d)). The main parameter accounting for the V_{loss}^{total} trend is ΔE_3; PM6:MYT (0.253 V), PM6:DYT (0.239 V), and PM6:TYT (0.231 V) (Table 3). The lowest V_{loss}^{total} of the PM6:TYT OSCs contributes to their highest V_{oc} (0.964 V) among the series.

The charge generation of each OSC was investigated by measuring its photocurrent density (J_{ph}) as a function of effective voltage (V_{eff}) (Fig. S15, ESI†).[63] The exciton dissociation probability ($P(E,T)$) of each OSC was calculated by dividing the J_{sc} by the saturated current density (J_{sat}) at V_{eff} = 2 V. The $P(E,T)$s of the OSCs were similarly high (~94%), indicating that the excitons dissociate well in all the blend systems. The charge transport of the OSCs was assessed by measuring the SCLC mobility of corresponding blend films (Fig. 3(e) and Table S5, ESI†). As the same PM6 donor was used, the hole mobilities (μ_hs) were comparable across all blend films ranging from 4.0 to 4.7 × 10^{-4} cm^2 V^{-1} s^{-1}. Interestingly, the trend in the μ_es of the blend films was consistent with the trend in the μ_es of their pristine acceptor constituents; *i.e.*, the μ_es of the blend films increased in the order of PM6:MYT (5.8 × 10^{-5} cm^2 V^{-1} s^{-1}) < PM6:DYT (3.8 × 10^{-4} cm^2 V^{-1} s^{-1}) < PM6:TYT (4.2 × 10^{-4} cm^2 V^{-1} s^{-1}) (Table S5, ESI†). The trend in the μ_es of the blend films is consistent with the trend in the J_{sc}s of the corresponding OSCs. Finally, the charge recombination of each OSC was investigated by measuring its light intensity (*P*)-dependent J_{sc} and V_{oc} (Fig. 3(f) and Fig. S16, Fig. ESI†). The slope (α) of the *P vs.* J_{sc} plots of the OSCs was similar (0.81–0.82), indicating that the OSCs experience similar degrees of bimolecular recombination (Fig. S16, ESI†).[64] However, the slope (*S*) of the *P vs.* V_{oc} plots of the OSCs differed; the *S* value associated with the PM6:TYT OSC (1.04 $kT\ q^{-1}$) was closer to 1 than those associated with the PM6:MYT and PM6:DYT OSCs (1.14 and 1.10 $kT\ q^{-1}$, respectively), indicating that monomolecular/trap-assisted recombination is more suppressed in the PM6:TYT OSC (Fig. 3(f)).[64] The suppressed monomolecular/trap-assisted recombination observed in the PM6:TYT OSC supports its comparatively high FF and low V_{loss}^{total} compared to the other OSCs.

Operational stability is another key requirement for the commercialization of OSCs. To investigate the long-term stability of the PM6:MYT, PM6:DYT, and PM6:TYT OSCs, we measured their PCE values under continuous 1 sun illumination (100 mW cm^{-2}) for 1080 h. Then, we estimated the $t_{80\%}$ lifetime of each device (*i.e.*, the time required for the PCE of the device to reach 80% of its initial PCE) by extrapolating the PCE of the device to that in longer illumination time (*i.e.*, 10 000 h) (Fig. 4(a)).[65–67] We note that the datapoints in Fig. 4(a) are the averaged values collected from three independent experiments for reliability. The stability test as well as the extrapolation procedures are described in the ESI.† The stability of the OSCs increased dramatically with increasing acceptor chain length (molecular size), based on the $t_{80\%}$ lifetimes of the PM6:MYT,

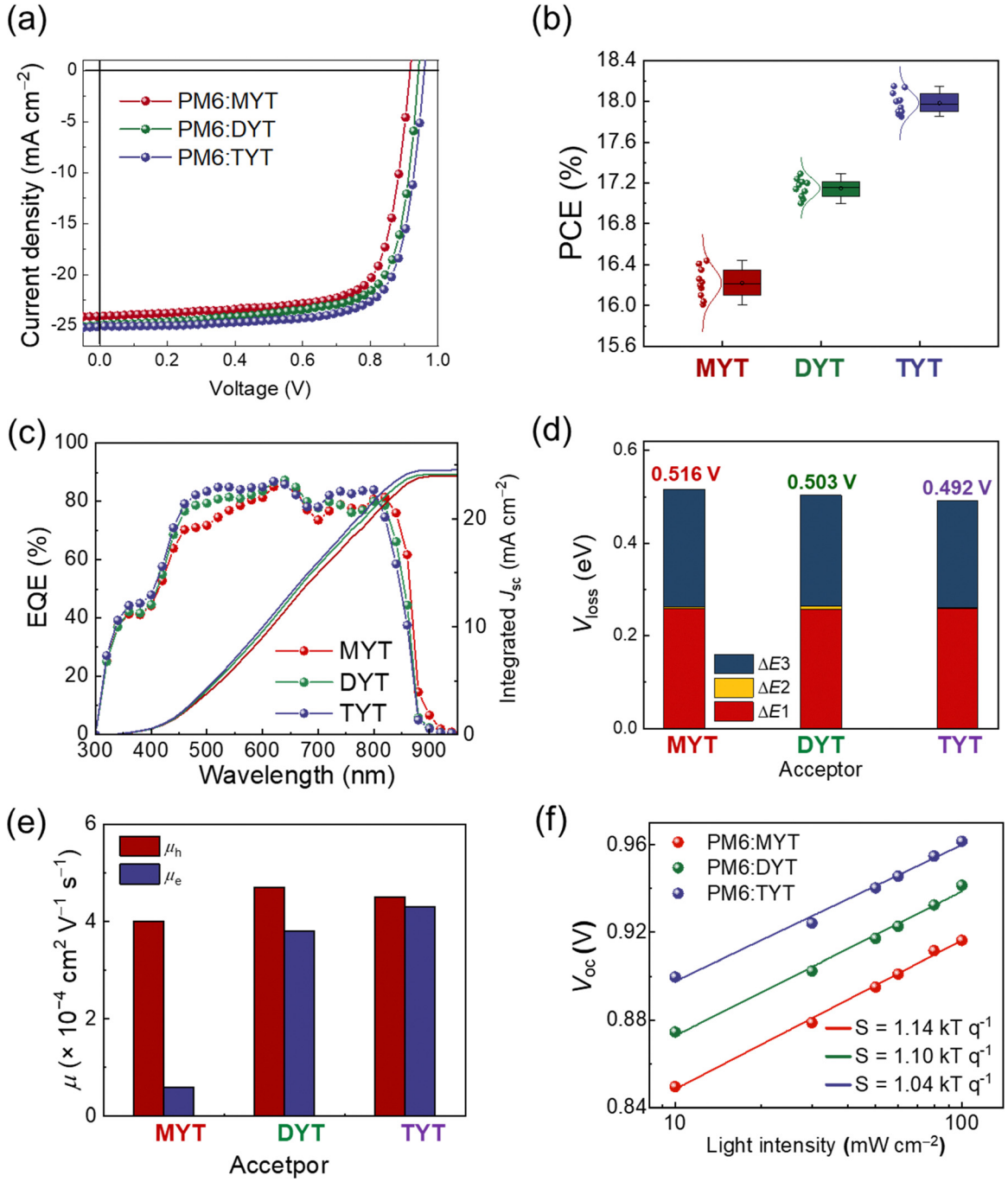

Fig. 3 (a) J–V curves, (b) PCE distributions, (c) EQE spectra, (d) V_{loss} parameters, (e) SCLC mobilities, and (f) light-intensity dependent V_{oc} plots of PM6:acceptor-based OSCs.

Table 2 Photovoltaic performances of PM6:acceptor OSCs

Acceptor	V_{oc} (V)	J_{sc} (mA cm^{-2})	Cal. J_{sc}[a] (mA cm^{-2})	FF	PCE$_{max(avg)}$[b] (%)
MYT	0.917	24.29	24.01	0.74	16.44 (16.22)
DYT	0.942	24.89	24.14	0.74	17.29 (17.15)
TYT	0.964	25.07	24.54	0.75	18.15 (17.98)

[a] Calculated from EQE spectra. [b] Average values obtained from 10 independent devices.

Table 3 Voltage loss parameters of PM6:acceptor OSCs

Acceptor	E_g (eV)	qV_{oc}^{SQ}	ΔE_1	qV_{oc}^{rad}	ΔE_2	qV_{oc}	ΔE_3	V_{loss}^{total}
MYT	1.433	1.174	0.259	1.170	0.004	0.917	0.253	0.516
DYT	1.447	1.187	0.258	1.181	0.006	0.942	0.239	0.503
TYT	1.458	1.197	0.259	1.195	0.002	0.964	0.231	0.492

PM6:DYT, and PM6:TYT OSCs which were 35, 2551, and 8454 h, respectively. It should be noted that the PM6:TYT demonstrates both high PCE (>18%) and high stability ($t_{80\%}$ lifetime > 8000 h) (Fig. 4(b) and Table S6, ESI†). To emphasize the excellent operational stability of the PM6:TYT OSCs, we estimated its device lifetime when operated in different locations (countries) considering the daily solar irradiance in each location.[66,68] The expected device lifetime of the PM6:TYT OSC was several years; 4.8 (Seoul), 7.2 (Paris), and 7.7 years (Berlin) (Table S7, ESI†). Additionally, we evaluated the thermal stability of the active layers at 80 °C (Fig. S17, ESI†). Each active layer was annealed before depositing the electron transporting layer, and the photovoltaic

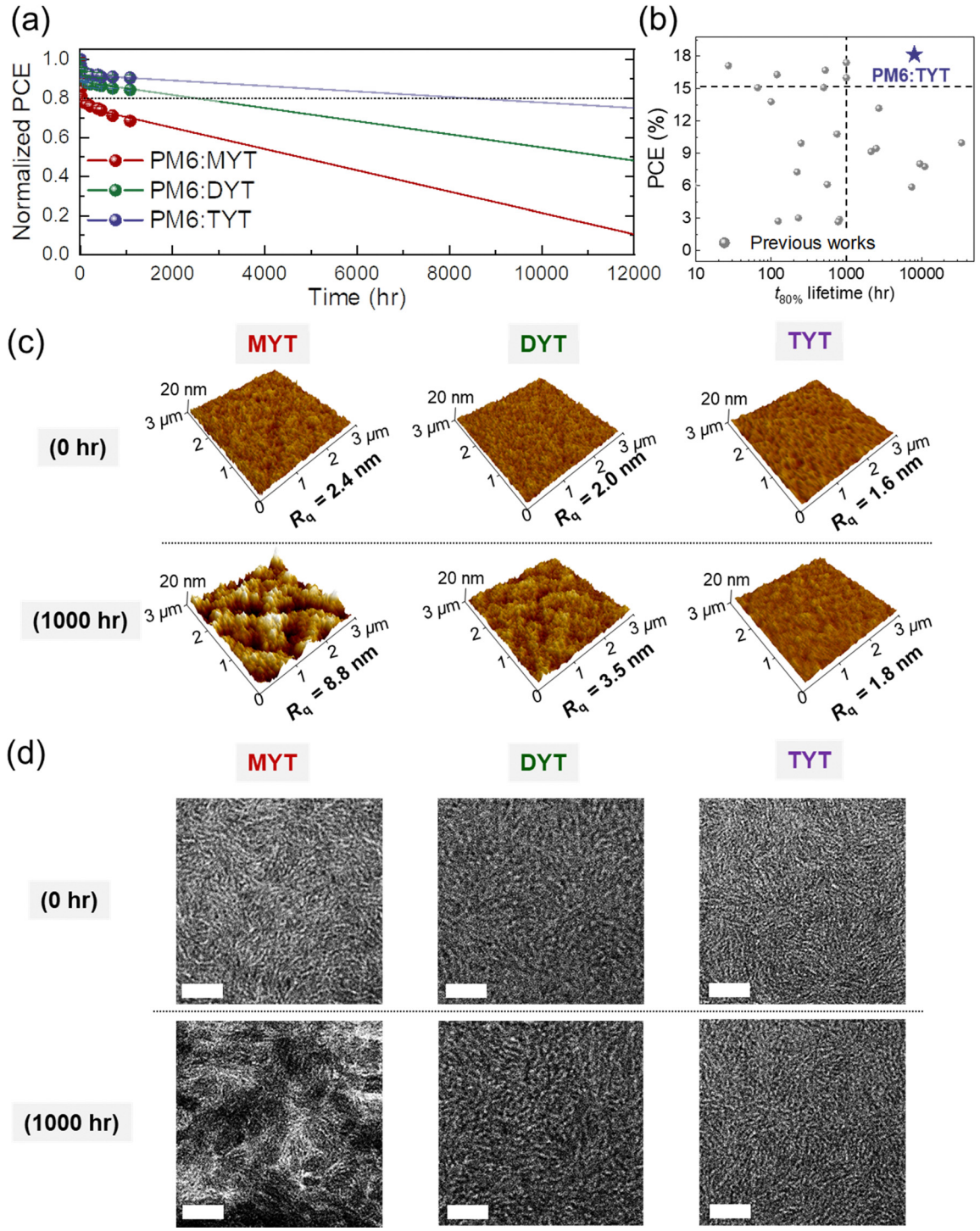

Fig. 4 (a) Normalized PCE of OSCs under continuous 1 sun illumination (100 mW cm^{-2}), (b) PCE *vs.* $t_{80\%}$ lifetime of previously reported OSCs and the PM6:TYT OSC, (c) AFM height and (d) TEM images of blend films (active layers) before and after 1000 h of illumination (scale bars are 50 nm).

performance of the fully assembled devices was examined. The thermal stability test exhibited a similar trend to that of the photo-stability test. For example, after 480 h of annealing, the normalized PCEs for the MYT-, DYT-, and TYT-based OSCs reached 76.2, 89.2, and 93.3% of their initial values, respectively.

The photo-stability of the OSCs can be affected by various intrinsic and extrinsic factors including metastable blend morphology, oxidation, diffusion of electrodes/interlayers, chemical degradation between the consisting layers, and trap-states of active components.[39,40,69] Particularly, change of the blend morphology under the light illumination is one of the most crucial factors that determine the operational stability of the OSCs.[16,69] To better understand the different operational stability of the OSCs, we examined the morphological stability of the blend films under 1 sun illumination. As the elevated temperature caused by the light illumination can provide strong thermal energy and accelerate the molecular motion and diffusion of the acceptor molecules, the photo-stability of OSCs is strongly related to the morphological stability of the active layer.[18,32,33] Therefore, we compared the blend films before and after 1000 h of illumination by atomic force microscopy (AFM) and transmission electron microscopy (TEM) (Fig. 4(c) and (d)). AFM revealed that the surface roughness of a PM6:MYT blend film increased over the course of 1000 h of illumination. In contrast, the surface roughness of a PM6:TYT blend film was almost unchanged. In detail, the root mean square roughness (R_q) of the PM6:MYT blend film increased from 2.4 to 8.8 nm after 1000 h of illumination, whereas that of the PM6:TYT blend film increased from 1.6 to 1.8 nm. The R_q of a PM6:DYT blend film increased from 2.0 to 3.5 nm after 1000 h of illumination (Fig. 4(c)). TEM revealed a similar trend; the PM6:MYT blend film experienced significantly greater phase separation during 1000 h illumination than the PM6:DYT and PM6:TYT blend films (Fig. 4(d)).

We analyzed the crystal structures in blend films before and after 1000 h of illumination by GIWAXS (Fig. 5(a)–(c) and Fig. S18, ESI†). The crystalline structures of a PM6:MYT blend film were significantly altered by illumination, as indicated by the appearance of many sharp scattering peaks after 1000 h in its

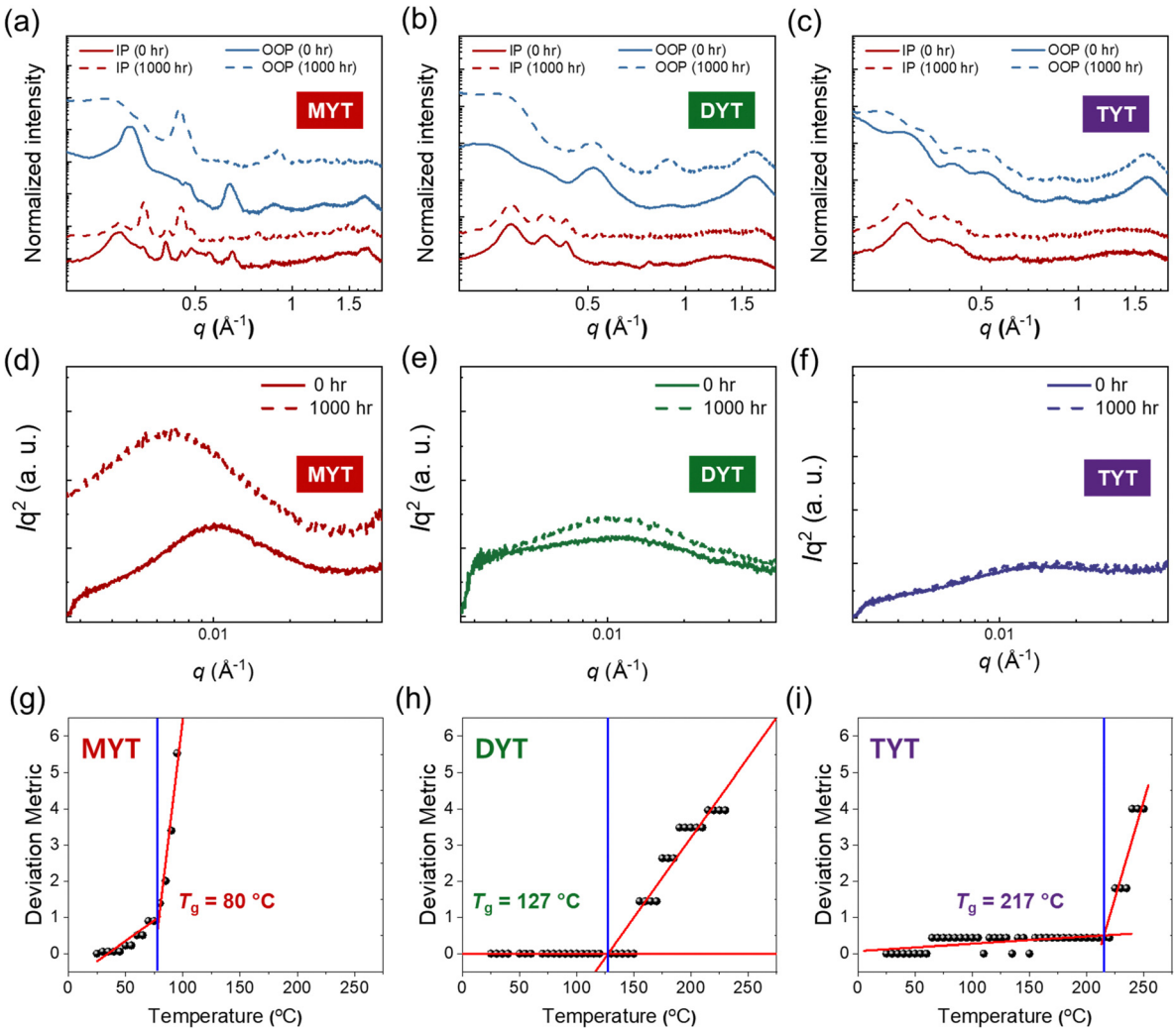

Fig. 5 (a)–(c) GIWAXS linecut profiles and (d)–(f) RSoXS patterns of (a), (d) PM6:MYT, (b), (e) PM6:DYT, and (c), (f) PM6:TYT blend films before and after 1000 h of illumination. (g)–(i) Plots of the DM_T of (g) MYT, (h) DYT, and (i) TYT films as a function of annealing temperature.

GIWAXS linecut profiles in the IP (q_{xy}: ~0.35 and ~0.45 Å^{-1}) and OOP directions (q_{xy}: ~0.45 and ~0.90 Å^{-1}) (Fig. 5(a)). In contrast, the crystal structures of PM6:DYT and PM6:TYT blend films were almost unaffected by illumination (Fig. 5(b)–(c)). The domain size and purity of the blend films were analyzed by resonant soft X-ray scattering (RSoXS) (Fig. 5(d)–(f) and Table S8, ESI†). A beam energy of 284.4 eV was used to maximize material contrast.[69] The RSoXS patterns of a PM6:MYT blend film before and after illumination showed that its domain size and relative domain purity (r-DP) significantly increased by irradiation, from 29 to 46 nm and 0.59 to 1.00, respectively. In contrast, the changes in the blend morphology of the PM6:DYT and PM6:TYT blends were not noticeable. The domain size and r-DP for the PM6:DYT blend increased from 30 to 31 nm and 0.47 to 0.52, while the domain size (25 nm) and r-DP (0.45) for the PM6:TYT blend were the same (Table S6, ESI†). We then conducted photoluminescence (PL) emission spectra measurements on both pristine acceptors and PM6:acceptor blend films to further examine the impact of illumination on blend morphology (Fig. S19, ESI†). Under continuous illumination, the PL quenching efficiencies (ηs) of the blend films rapidly decreased in the PM6:MYT blend film, whereas the η values remained nearly constant in the PM6:TYT blend film. For instance, after 24 h of illumination, the decrease in η values for the blend films is in the order of PM6:TYT blend films (93.8 → 93.3%), PM6:DYT (93.4 → 85.6%), and PM6:MYT (94.7 → 60.8%). This finding is consistent with the above results, indicating that the photo-stability of the blend films significantly increased in the order of PM6:MYT, PM6:DYT, and PM6:TYT.

The photo-stable blend morphology and device performance of the PM6:TYT OSC are mainly attributed to the relatively large molecular size of TYT and the related physical properties including the T_g and molecular diffusivity. To determine the correlation between the molecular size of the acceptor and its diffusivity, we estimated the T_gs of the acceptors by measuring their UV-Vis absorbance in film at various annealing temperatures (20–240 °C) (Fig. S20, ESI†). The T_g of SMAs corresponds to an onset temperature for thermal-induced molecular motions and diffusions, at which the SMAs start to be significantly mobile and imperfect SMA crystals are reorganized.[16,69] Thus, the estimated T_gs of the SMAs can be also affected by their kinetically trapped morphologies in film in addition to the intrinsic molecular properties. To precisely correlate the estimated T_gs of the acceptors with those in the OSC device, we applied the same processing conditions used in the OSC fabrication to prepare the films for T_g measurements. A deviation metric (DM_T), quantifying the change in the UV-Vis absorbance of each film during annealing, was used to estimate the T_gs of the acceptor films (Fig. 5(g)–(i)).[16,70,71] Details of the procedure are provided in the ESI.† The T_gs of the acceptors increased with increasing molecular size; the T_gs of MYT, DYT, and TYT were 80, 127, and 217 °C, respectively. Based on the T_gs of the acceptors, we estimated their D values in the blend films with the PM6 donor at 85 °C using a previously reported approach.[72] The D_{85}s of the acceptors decreased with increasing T_gs (and molecular size); *i.e.*, in the order of MYT (D_{85}: 1.2 × 10^{-16} cm^2 s^{-1}), DYT (D_{85}: 1.1 × 10^{-19} cm^2 s^{-1}), and TYT (D_{85}: 1.4 × 10^{-25} cm^2 s^{-1}). In addition, the D_{85} of TYT was 10^6–10^9 of magnitude lower than those of the other reported high-performance acceptor materials (D_{85} = 10^{-19}–10^{-16} cm^2 s^{-1}).[16,72] As a result, the diffusion time of the acceptor molecules to move 10 nm ($t_D^{10\,nm}$) at 85 °C in the PM6:acceptor blends increased in the order of MYT ($t_D^{10\,nm}$: 2.3 × 10^0 h), DYT ($t_D^{10\,nm}$: 2.7 × 10^3 h), and TYT ($t_D^{10\,nm}$: 1.9 × 10^9 h) (Table 4).[73,74] Moreover, D_{120} values measured by time-of-flight secondary ion mass spectrometry (ToF-SIMS) profiles of PM6:acceptors bilayers demonstrated the same trend, exhibiting a progressive decrease in the diffusion coefficient within the donor matrix as molecular size increases (Fig. S21 and Table S9, ESI†). Therefore, the high T_g (217 °C) and lower D_{85} (1.4 × 10^{-25} cm^2 s^{-1}) of TYT, relative to those of MYT (T_g = 80 °C and D_{85} = 1.2 × 10^{-16} cm^2 s^{-1}) account for the excellent operational stability of the PM6:TYT OSCs.

Table 4 $t_{80\%}$ lifetimes of PM6:acceptor OSCs and the T_gs and D_{85}s of acceptors

Acceptor	$t_{80\%}$ lifetime[a] (h)	T_g[b] (°C)	D_{85}[c] (cm^2 s^{-1})	$t_D^{10\,nm}$[d] (h)
MYT	35	80	1.2 × 10^{-16}	2.3 × 10^0
DYT	2551	127	1.1 × 10^{-19}	2.7 × 10^3
TYT	8454	217	1.4 × 10^{-25}	1.9 × 10^9

[a] Estimated from OSC stability test results under 1 sun illumination. [b] Estimated from DM_T *vs.* temperature plots. [c] D of the acceptor in a blend with PM6 at 85 °C, D_{85} = 1.2 × 10^7 × exp(−0.15 × T_g). [d] Diffusion time to move a 10 nm distance at 85 °C in a blend with PM6; $t_D = L^2 \times D_{85}^{-1}$; L = diffusion length.

Conclusions

We developed an efficient (PCE = 18.15%) and highly stable ($t_{80\%}$ lifetime = 8454 h) OSC by designing a novel non-fullerene trimer acceptor, TYT, blended with PM6 to form the active layer. TYT consists of three Y-series-based molecules linked by two thiophene spacers and it was found to have a higher LUMO energy level than the corresponding monomer and dimer acceptors (MYT and DYT, respectively) owing to the electron-donating nature of the two thiophene spacers. As a result, the V_{oc} and PCE of a PM6:TYT OSC (0.964 V and 18.15%, respectively) exceeded those of a PM6:MYT OSC (0.917 V and 16.44%, respectively) as well as a PM6:DYT OSC (0.942 V and 17.29%, respectively). Importantly, TYT had an extremely high T_g (217 °C) and low D_{85} (1.4 × 10^{-25} cm^2 s^{-1}) owing to its relatively large molecular size, which, in turn, imparted greater operational stability to a resulting OSC. Accordingly, the operational stability of a PM6:TYT OSC ($t_{80\%}$ lifetime = 8454 h) significantly exceeded that of PM6:MYT ($t_{80\%}$ lifetime = 35 h) and PM6:DYT OSCs ($t_{80\%}$ = 2551 h). We expect that the molecular structure–acceptor property–device performance relationship established in this study provides important design guidelines for the acceptor materials for producing OSCs with high V_{oc} and excellent device stability.

Conflicts of interest

There are no conflicts to declare.

Acknowledgements

This work was supported by the National Research Foundation of Korea (NRF-2017M3A7B8065584, 2022R1A2B5B03001761, 2022M3J7A1062940, 2019R1A6A1A11053838, and 2022M3C1A-3081211). This research used resources of the Advanced Light Source, which is a DOE Office of Science User Facility under contract no. DE-AC02-05CH11231.

References

1 C. Li, J. D. Zhou, J. L. Song, J. Q. Xu, H. T. Zhang, X. N. Zhang, J. Guo, L. Zhu, D. H. Wei, G. C. Han, J. Min, Y. Zhang, Z. Q. Xie, Y. P. Yi, H. Yan, F. Gao, F. Liu and Y. M. Sun, *Nat. Energy*, 2021, **6**, 605–613.

2 J. Yuan, Y. Q. Zhang, L. Y. Zhou, G. C. Zhang, H. L. Yip, T. K. Lau, X. H. Lu, C. Zhu, H. J. Peng, P. A. Johnson, M. Leclerc, Y. Cao, J. Ulanski, Y. F. Li and Y. P. Zou, *Joule*, 2019, **3**, 1140–1151.

3 J.-W. Lee, C. Lim, S. W. Lee, Y. Jeon, S. Lee, T. S. Kim, J. Y. Lee and B. J. Kim, *Adv. Energy Mater.*, 2022, **12**, 2202224.

4 H. Y. Chen, R. Zhang, X. B. Chen, G. Zeng, L. Kobera, S. Abbrent, B. Zhang, W. J. Chen, G. Y. Xu, J. Oh, S. H. Kang, S. S. Chen, C. Yang, J. Brus, J. H. Hou, F. Gao, Y. W. Li and Y. F. Li, *Nat. Energy*, 2021, **6**, 1045–1053.

5 Y. H. Cai, Y. Li, R. Wang, H. B. Wu, Z. H. Chen, J. Zhang, Z. F. Ma, X. T. Hao, Y. Zhao, C. F. Zhang, F. Huang and Y. M. Sun, *Adv. Mater.*, 2021, **33**, 2101733.

6 G. U. Kim, C. Sun, J. S. Park, H. G. Lee, D. Lee, J.-W. Lee, H. J. Kim, S. Cho, Y. H. Kim, S. K. Kwon and B. J. Kim, *Adv. Funct. Mater.*, 2021, **31**, 2100870.

7 J.-W. Lee, S. Seo, S.-W. Lee, G.-U. Kim, S. Han, T. N.-L. Phan, S. Lee, S. Li, T.-S. Kim, J.-Y. Lee and B. J. Kim, *Adv. Mater.*, 2022, **34**, 2207544.

8 J. H. Hou, O. Inganas, R. H. Friend and F. Gao, *Nat. Mater.*, 2018, **17**, 119–128.

9 S. X. Li, L. L. Zhan, Y. Z. Jin, G. Q. Zhou, T. K. Lau, R. Qin, M. M. Shi, C. Z. Li, H. M. Zhu, X. H. Lu, F. L. Zhang and H. Z. Chen, *Adv. Mater.*, 2020, **32**, 2001160.

10 C. L. He, Y. W. Pan, Y. N. Ouyang, Q. Shen, Y. Gao, K. R. Yan, J. Fang, Y. Y. Chen, C. Q. Ma, J. Min, C. F. Zhang, L. J. Zuo and H. Z. Chen, *Energy Environ. Sci.*, 2022, **15**, 2537–2544.

11 J.-W. Lee, D. Jeong, D. J. Kim, T. N.-L. Phan, J. S. Park, T.-S. Kim and B. Kim, *Energy Environ. Sci.*, 2021, **14**, 4067–4076.

12 Q. P. Fan, W. Y. Su, S. S. Chen, W. Kim, X. B. Chen, B. Lee, T. Liu, U. A. Mendez-Romero, R. J. Ma, T. Yang, W. L. Zhuang, Y. Li, Y. W. Li, T. S. Kim, L. T. Hou, C. Yang, H. Yan, D. H. Yu and E. G. Wang, *Joule*, 2020, **4**, 658–672.

13 J.-W. Lee, B. S. Ma, H. J. Kim, T.-S. Kim and B. J. Kim, *JACS Au*, 2021, **1**, 612–622.

14 K. E. Hung, Y. S. Lin, Y. J. Xue, H. R. Yang, Y. Y. Lai, J. W. Chang, C. J. Su, A. C. Su, C. S. Hsu, U. S. Jeng and Y. J. Cheng, *Adv. Energy Mater.*, 2022, **12**, 2103702.

15 J.-W. Lee, B. S. Ma, J. Choi, J. Lee, S. Lee, K. Liao, W. Lee, T. S. Kim and B. J. Kim, *Chem. Mater.*, 2020, **32**, 582–594.

16 Y. P. Qin, N. Balar, Z. X. Peng, A. Gadisa, I. Angunawela, A. Bagui, S. Kashani, J. H. Hou and H. Ade, *Joule*, 2021, **5**, 2129–2147.

17 J.-W. Lee, C. Sun, D. J. Kim, M. Y. Ha, D. Han, J. S. Park, C. Wang, W. B. Lee, S.-K. Kwon, T.-S. Kim, Y.-H. Kim and B. J. Kim, *ACS Nano*, 2021, **15**, 19970–19980.

18 M. Ghasemi, H. W. Hu, Z. X. Peng, J. J. Rech, I. Angunawela, J. H. Carpenter, S. J. Stuard, A. Wadsworth, I. McCulloch, W. You and H. Ade, *Joule*, 2019, **3**, 1328–1348.

19 J. B. Zhang, C. H. Tan, K. Zhang, T. Jia, Y. J. Cui, W. Y. Deng, X. F. Liao, H. B. Wu, Q. H. Xu, F. Huang and Y. Cao, *Adv. Energy Mater.*, 2021, **11**, 2102559.

20 J.-W. Lee, C. Sun, B. S. Ma, H. J. Kim, C. Wang, J. M. Ryu, C. Lim, T. S. Kim, Y. H. Kim, S. K. Kwon and B. J. Kim, *Adv. Energy Mater.*, 2021, **11**, 2003367.

21 Q. P. Fan, W. Y. Su, S. S. Chen, T. Liu, W. L. Zhuang, R. J. Ma, X. Wen, Z. H. Yin, Z. H. Luo, X. Guo, L. T. Hou, K. Moth-Poulsen, Y. Li, Z. G. Zhang, C. Yang, D. H. Yu, H. Yan, M. J. Zhang and E. G. Wang, *Angew. Chem., Int. Ed.*, 2020, **59**, 19835–19840.

22 Y. Li, J. L. Song, Y. C. Dong, H. Jin, J. M. Xin, S. J. Wang, Y. H. Ca, L. Jiang, W. Ma, Z. Tang and Y. M. Sun, *Adv. Mater.*, 2022, **34**, 2110155.

23 J.-W. Lee, S. W. Lee, J. Kim, Y. H. Ha, C. Sun, T. N. L. Phan, S. Lee, C. Wang, T. S. Kim, Y. H. Kim and B. J. Kim, *J. Mater. Chem. A*, 2022, **10**, 20312–20322.

24 Z. Genene, J.-W. Lee, S.-W. Lee, Q. Chen, Z. Tan, B. A. Abdulahi, D. Yu, T.-S. Kim, B. J. Kim and E. Wang, *Adv. Mater.*, 2022, **34**, 2107361.

25 B. Liu, H. L. Sun, J.-W. Lee, J. Yang, J. W. Wang, Y. C. Li, B. B. Li, M. Xu, Q. G. Liao, W. Zhang, D. X. Han, L. Niu, H. Meng, B. J. Kim and X. G. Guo, *Energy Environ. Sci.*, 2021, **14**, 4499–4507.

26 J.-W. Lee, C. Sun, S. W. Lee, G. U. Kim, S. Li, C. Wang, T. S. Kim, Y. H. Kim and B. J. Kim, *Energy Environ. Sci.*, 2022, **15**, 4672–4685.

27 H. Yu, Y. Wang, H. Kim, X. Wu, Y. H. Li, Z. F. Yao, M. G. Pan, X. H. Zou, J. Q. Zhang, S. S. Chen, D. H. Zhao, F. Huang, X. H. Lu, Z. L. Zhu and H. Yan, *Adv. Mater.*, 2022, **34**, 2200361.

28 C. Sun, J.-W. Lee, S. Seo, S. Lee, C. Wang, H. Li, Z. P. Tan, S. K. Kwon, B. J. Kim and Y. H. Kim, *Adv. Energy Mater.*, 2022, **12**, 2103239.

29 H. L. Sun, B. Liu, Y. L. Ma, J.-W. Lee, J. Yang, J. W. Wang, Y. C. Li, B. B. Li, K. Feng, Y. Q. Shi, B. H. Zhang, D. X. Han, H. Meng, L. Niu, B. J. Kim, Q. D. Zheng and X. G. Guo, *Adv. Mater.*, 2021, **33**, 2102635.

30 S. Seo, C. Sun, J.-W. Lee, S. Lee, D. Lee, C. Wang, T. N. L. Phan, G.-U. Kim, S. Cho, Y. H. Kim and B. J. Kim, *Adv. Funct. Mater.*, 2022, **32**, 2108508.

31 G. Zeng, W. J. Chen, X. B. Chen, Y. Hu, Y. Chen, B. Zhang, H. Y. Chen, W. W. Sun, Y. X. Shen, Y. W. Li, F. Yan and Y. F. Li, *J. Am. Chem. Soc.*, 2022, **144**, 8658–8668.

32 Y. Chen, J. Y. Wan, G. Y. Xu, X. X. Wu, X. Q. Li, Y. X. Shen, F. Yang, X. M. Ou, Y. W. Li and Y. F. Li, *Sci. China: Chem.*, 2022, **65**, 1164–1172.

33 B. Zhang, F. Yang, S. S. Chen, H. Y. Chen, G. Zeng, Y. X. Shen, Y. W. Li and Y. F. Li, *Adv. Funct. Mater.*, 2022, **32**, 2202011.
34 L. L. Zhang, Z. Q. Zhang, D. Deng, H. Q. Zhou, J. Q. Zhang and Z. X. Wei, *Adv. Sci.*, 2022, 2202513.
35 Y. C. Liang, D. F. Zhang, Z. R. Wu, T. Jia, L. Luer, H. R. Tang, L. Hong, J. B. Zhang, K. Zhang, C. J. Brabec, N. Li and F. Huang, *Nat. Energy*, 2022, **7**, 1180–1190.
36 S. Li, R. Zhang, M. Zhang, J. Yao, Z. Peng, Q. Chen, C. Zhang, B. Chang, Y. Bai, H. Fu, Y. Ouyang, C. Zhang, J. A. Steele, T. Alshahrani, M. B. J. Roeffaers, E. Solano, L. Meng, F. Gao, Y. Li and Z.-G. Zhang, *Adv. Mater.*, 2022, 2206563, DOI: **10.1002/adma.202206563,**.
37 H. T. Wang, C. C. Cao, H. Chen, H. J. Lai, C. X. Ke, Y. L. Zhu, H. Li and F. He, *Angew. Chem., Int. Ed.*, 2022, **61**, e202201844.
38 J. Lee, R. Singh, D. H. Sin, H. G. Kim, K. C. Song and K. Cho, *Adv. Mater.*, 2016, **28**, 69–76.
39 Y. Z. Lin, Y. F. Wang, J. Y. Wang, J. H. Hou, Y. F. Li, D. B. Zhu and X. W. Zhan, *Adv. Mater.*, 2014, **26**, 5137–5142.
40 Y. Z. Lin, J. Y. Wang, S. X. Dai, Y. F. Li, D. B. Zhu and X. W. Zhan, *Adv. Energy Mater.*, 2014, **4**, 1400420.
41 J. Liu, S. S. Chen, D. P. Qian, B. Gautam, G. F. Yang, J. B. Zhao, J. Bergqvist, F. L. Zhang, W. Ma, H. Ade, O. Inganas, K. Gundogdu, F. Gao and H. Yan, *Nat. Energy*, 2016, **1**, 16089.
42 Q. Burlingame, M. Ball and Y. L. Loo, *Nat. Energy*, 2020, **5**, 947–949.
43 P. Cheng and X. W. Zhan, *Chem. Soc. Rev.*, 2016, **45**, 2544–2582.
44 W. Y. Yang, W. Wang, Y. H. Wang, R. Sun, J. Guo, H. N. Li, M. M. Shi, J. Guo, Y. Wu, T. Wang, G. H. Lu, C. J. Brabec, Y. F. Li and J. Min, *Joule*, 2021, **5**, 1209–1230.
45 Y. Zhong, B. Kumar, S. Oh, M. T. Trinh, Y. Wu, K. Elbert, P. P. Li, X. Y. Zhu, S. X. Xiao, F. Ng, M. L. Steigerwald and C. Nuckolls, *J. Am. Chem. Soc.*, 2014, **136**, 8122–8130.
46 G. Y. Zhang, J. B. Zhao, P. C. Y. Chow, K. Jiang, J. Q. Zhang, Z. L. Zhu, J. Zhang, F. Huang and H. Yan, *Chem. Rev.*, 2018, **118**, 3447–3507.
47 N. N. Liang, K. Sun, Z. Zheng, H. F. Yao, G. P. Gao, X. Y. Meng, Z. H. Wang, W. Ma and J. H. Hou, *Adv. Energy Mater.*, 2016, **6**, 1600060.
48 Y. W. Duan, X. P. Xu, H. Yan, W. L. Wu, Z. J. Li and Q. Peng, *Adv. Mater.*, 2017, **29**, 1605115.
49 P. Cheng, X. G. Zhao and X. W. Zhan, *Acc. Mater. Res.*, 2022, **3**, 309–318.
50 N. N. Liang, D. Meng and Z. H. Wang, *Acc. Chem. Res.*, 2021, **54**, 961–975.
51 Y. Z. Lin and X. W. Zhan, *Acc. Chem. Res.*, 2016, **49**, 175–183.
52 N. K. Elumalai and A. Uddin, *Energy Environ. Sci.*, 2016, **9**, 391–410.
53 D. P. Qian, Z. L. Zheng, H. F. Yao, W. Tress, T. R. Hopper, S. L. Chen, S. S. Li, J. Liu, S. S. Chen, J. B. Zhang, X. K. Liu, B. W. Gao, L. Q. Ouyang, Y. Z. Jin, G. Pozina, I. A. Buyanova, W. M. Chen, O. Inganas, V. Coropceanu, J. L. Bredas, H. Yan, J. H. Hou, F. L. Zhang, A. A. Bakulin and F. Gao, *Nat. Mater.*, 2018, **17**, 703–709.
54 L. L. Zhan, S. X. Li, Y. K. Li, R. Sun, J. Min, Z. Z. Bi, W. Ma, Z. Chen, G. Q. Zhou, H. M. Zhu, M. M. Shi, L. J. Zuo and H. Z. Chen, *Joule*, 2022, **6**, 662–675.
55 T. L. Nguyen, T. H. Lee, B. Gautam, S. Y. Park, K. Gundogdu, J. Y. Kim and H. Y. Woo, *Adv. Funct. Mater.*, 2017, **27**, 1702474.
56 K. Kawashima, Y. Tamai, H. Ohkita, I. Osaka and K. Takimiya, *Nat. Commun.*, 2015, **6**, 10085.
57 S. Natsuda, T. Saito, R. Shirouchi, Y. Sakamoto, T. Takeyama, Y. Tamai and H. Ohkita, *Energy Environ. Sci.*, 2022, **15**, 1545–1555.
58 Z. Chiguvare and V. Dyakonov, *Phys. Rev. B: Condens. Matter Mater. Phys.*, 2004, **70**, 235207.
59 Y. L. Ma, M. Zhang, S. Wan, P. Yin, P. S. Wang, D. D. Cai, F. Liu and Q. D. Zheng, *Joule*, 2021, **5**, 197–209.
60 H. B. Naveed, K. Zhou and W. Ma, *Acc. Chem. Res.*, 2019, **52**, 2904–2915.
61 X. K. Chen, D. P. Qian, Y. M. Wang, T. Kirchartz, W. Tress, H. F. Yao, J. Yuan, M. Hulsbeck, M. J. Zhang, Y. P. Zou, Y. M. Sun, Y. F. Li, J. H. Hou, O. Inganas, V. Coropceanu, J. L. Bredas and F. Gao, *Nat. Energy*, 2021, **6**, 799–806.
62 T. M. Clarke and J. R. Durrant, *Chem. Rev.*, 2010, **110**, 6736–6767.
63 P. W. M. Blom, V. D. Mihailetchi, L. J. A. Koster and D. E. Markov, *Adv. Mater.*, 2007, **19**, 1551–1566.
64 S. R. Cowan, A. Roy and A. J. Heeger, *Phys. Rev. B: Condens. Matter Mater. Phys.*, 2010, **82**, 245207.
65 Q. Burlingame, X. H. Huang, X. Liu, C. Jeong, C. Coburn and S. R. Forrest, *Nature*, 2019, **573**, 394–397.
66 X. Y. Du, T. Heumueller, W. Gruber, A. Classen, T. Unruh, N. Li and C. J. Brabec, *Joule*, 2019, **3**, 215–226.
67 X. Xu, J. Y. Xiao, G. C. Zhang, L. Wei, X. C. Jiao, H. L. Yip and Y. Cao, *Sci. Bull.*, 2020, **65**, 208–216.
68 PVWatts Calculator. Solar Resource Data, **https://pvwatts.nrel.gov/pvwatts.php**, National Renewable Energy Laboratory, 2022, (accessed November 2022).
69 J.-W. Lee, G.-U. Kim, D. J. Kim, Y. Jeon, S. Li, T. S. Kim, J. Y. Lee and B. J. Kim, *Adv. Energy Mater.*, 2022, **12**, 2200887.
70 S. E. Root, M. A. Alkhadra, D. Rodriquez, A. D. Printz and D. J. Lipomi, *Chem. Mater.*, 2017, **29**, 2646–2654.
71 D. Han, Y. Han, Y. Kim, J.-W. Lee, D. Jeong, H. Park, G.-U. Kim, F. S. Kim and B. J. Kim, *J. Mater. Chem. A*, 2022, **10**, 640–650.
72 M. Ghasemi, N. Balar, Z. X. Peng, H. W. Hu, Y. P. Qin, T. Kim, J. J. Rech, M. Bidwell, W. Mask, I. McCulloch, W. You, A. Amassian, C. Risko, B. T. O'Connor and H. Ade, *Nat. Mater.*, 2021, **20**, 525–532.
73 M. T. Sajjad, A. Ruseckas and I. D. W. Samuel, *Matter*, 2020, **3**, 341–354.
74 S. M. Menke and R. J. Holmes, *Energy Environ. Sci.*, 2014, **7**, 499–512.